Proceedings of the 6^{th} International Conference on Fluid Flow and Thermal Science (ICFFTS 2025)

Barcelona, Spain - October 29 - 31, 2025

Paper No. 136

DOI: 10.11159/icffts25.136

Impact of Manifold Inlet/Outlet Positioning On the Thermohydraulic Efficiency of a Topology-Optimized Pin Fin Heat Sink: Thermal Management of Evs

Nima Mazaheri¹, Aggrey Mwsiegey²

¹Department of Mechanical and Manufacturing Engineering, Schulich School of Engineering, University of Calgary, 2500 University Drive NW, Calgary, AB, T2N 1N4, Canada

nima.mazaheri@ucalgary.ca; aggrey.mwesigye@ucalgary.ca

Abstract - This investigation focuses on the impact of manifold location on the thermal and hydraulic attributes of a topology-optimized pin fin heat sink for thermal management of high heat flux IGBTs (insulated gate bipolar transistors), particularly in power inverters of electric and hybrid vehicles. The numerical simulations are carried out for four distinct manifold locations, including single inlet/outlet manifold designs labelled M— and N—, and U-shaped, plus a new manifold named Dual. Water is used as a coolant with a mass flow rate ranging from 0.25 kg/s to 1 kg/s and the IGBT heat flux of 200 W/cm². The cooling target is the well-known Toyota Prius power inverter module. To this end, ANSYS Fluent is employed and modelling the turbulent flow is accomplished using the four-equation SST model to improve accuracy. The numerical technique is verified and validated by available experimental results. The outcomes revealed that using the new dual manifold results in a 43% superior heat transfer compared to the N—shaped one, which is almost twice that of the M-shaped manifold. Thanks to the superior cooling efficiency achieved by the new Dual manifold design, the average and maximum IGBT temperatures drop by 13°C and 29°C, respectively. It was found that the new Dual manifold not only increases the heat transfer and results in a lower IGBT temperature but also enhances the temperature uniformity by 75% which has a key impact on the longevity and reliability of the IGBTs and the power inverter. The higher cooling capability of the new Dual manifold is obtained at the expense of a 119% increase in pumping power; however, considering constant pumping power, the new Dual design outperforms its counterparts. At a constant pumping power of 13.5 W, the Dual design improves the temperature uniformity by 71% compared to the N—shaped one.

Keywords: Thermal management of EVs, electronics cooling, IGBT, high-heat flux, manifold design, topology optimized heat sink

1. Introduction

Today, the adoption of electric and hybrid vehicles is a crucial strategy for reducing transportation-related emissions and aligning with climate objectives [1]. According to the International Energy Agency (IEA), the net savings from transitioning to electric and hybrid vehicles compared to internal combustion engine vehicles are estimated to be nearly 580 million tons of CO₂ in 2022 on a well-to-wheel basis [2]. Despite the rapid growth in electric vehicle adoption, the technology remains relatively immature and faces significant thermal management challenges in both vehicles and charging stations. Excessive heat accumulation limits the driving range and reduces energy efficiency, while high-power fast charging degrades heat dissipation in electrical components, particularly semiconductor devices. If not properly managed, overheating can lead to efficiency losses, reduced lifespan, and catastrophic device failure [3]. The limited heat dissipation of the current commercialized cooling technologies [4] and expecting heat dissipation of 500-1000 W/cm² for future high-power electronics (HPEs) in EVs and HVs [5], necessitates advanced thermal management solutions to meet the current and future cooling requirements. The persistent issue of overheating in Tesla inverters across various models [6], including the latest Model S [7], as reported in multiple forums, underscores an ongoing challenge in thermal management [8] that must be addressed. The solution lies in the implementation of highly efficient power electronics components with novel thermal management strategies, specifically for the inverters, which hold a pivotal responsibility in enhancing the overall energy efficiency of the EV [9,10]. Challenges in EV and HVs thermal management are especially pronounced in mid-sized and heavy-duty EVs, which generate significant heat due to their larger battery capacities and higher power demands.

To provide cooling for the increasing heat fluxes in power electronics components of EVs and hybrid EVs, a cooling mechanism with heat transfer rates beyond those achievable with current heat sinks is important. Novel heat sinks combining

more than one approach, such as jet impingement with microchannel heat sinks, among others, are emerging as means of removing extremely high amounts of heat in high heat flux electronic components [11]. Other mechanisms include optimizing heat sinks for specific heat fluxes in diverse applications.

Employing pin-fins is a popular heat transfer technique due to their advantages over conventional heat sinks, including higher heat transfer coefficients and lower thermal resistance [12]. In addition, pin-fin heat sinks can accommodate different geometries and configurations of the pins, such as circular, elliptical, airfoiled, conical, wavy, prism, etc., to optimize the thermal and hydraulic performance [12]. Pin-fin heat sinks exhibit a wide range of applications, serving as effective cooling solutions for various electronic equipment, high-power LED chips, and more. They are also utilized for cooling semiconductor lasers and phased array radars, making them versatile and indispensable in diverse technological fields [13]. Han et al. [14] researched an integrated design of a liquid-cooled heat sink for a 30-kW motor inverter in electric vehicles, considering the distribution of power devices. The authors identified the limitations of using commercial-off-the-shelf cold plate heat sinks and proposed three different configurations of heat sinks, comparing their cooling performance using numerical simulations and experiments. The authors concluded that taking into account both the pressure loss and the temperature, the optimum values for the inlet flow rate and the fin thickness are respectively 3 L/min and 1.2 mm. Zhao et al. [15] investigated the effects of different triangular pin-fin shapes on the cooling performance of a minichannel heat sink for IGBT modules through numerical analysis. The authors compared four different pin-fin configurations and reported that the equilateral triangular pin-fin has the best thermal and hydraulic attributes. They also proposed a method to optimize the pin-fin angle design based on the Nusselt number and friction factor. Moreover, their results suggest using a rotation angle close to 120° to improve cooling efficiency. Of each al. [16] parametrically studied the impact of the numbers, thicknesses, and heights of straight fins in the liquid cooling plate on both cooling performance and pressure drop for cooling of IGBT modules. The authors proposed seven types of fins to further enhance the cooling attributes of the IGBT modules. The introduction of the seven newly designed fins resulted in a notable decrease of 3-8 K in the maximum temperature of the cold plate. However, the trade-off was that these fins exhibited a significant increase in pressure drop. Eventually, the authors discovered that arc-shaped protruding fins were the optimal choice, exhibiting 6.2 K lower maximum temperature and 3.3 K lower average temperature, with a 2 times higher pressure drop compared to basic straight fins.

The current investigation provides a comprehensive analysis of the effects of manifold positioning on the thermal and hydraulic attributes of water within a topology-optimized pin fin heat sink for cooling of IGBTs within power inverters of EVs/HVs. A rigorous numerical approach was employed, utilizing the ANSYS FLUENT software, which was thoroughly verified and validated to ensure the accuracy of the results. The simulations were conducted under various conditions, including four distinct manifold locations and multiple flow rates, allowing for a thorough examination of the manifold location's impact on key parameters such as the Nusselt number, IGBT maximum temperature, temperature uniformity, and pumping power. By investigating these factors, this study makes a significant contribution to the development of sustainable transportation solutions and the advancement of electric mobility by improving the thermal management of high-heat flux components in EVs/HVs.

2. Definition of heat sinks

The fin heat sinks under study include pin fin heat sinks equipped with novel topology-optimized pin fins. The special shapes of the pin fins were acquired by implementing a multi-objective topology optimization, and it was demonstrated that this pin fin shape outperforms the circular-shaped pin fins. The focus of this contribution is on the manifold's impact on the thermohydraulic features of the coolant. Fig. 1 demonstrates pin-fin heat sinks with different manifold locations. The manifold locations are selected based on common manifold designs in industry. The heat sink's dimensions are 146 mmx 123 mmx 23 mm with the baseplate thickness of 6 mm. As these heat sinks are specifically designed for cooling IGBT modules in motor inverters of EVs and HVs, they can accommodate up to 6 IGBTs with the standard gap distance. The rationale behind this special pin fin arrangement, known as a targeted arrangement, is to ensure that each IGBT is delivered with sufficient cooling performance while keeping the pressure drop as low as possible. The heat sink is made of aluminum with a thermal conductivity of 152 W/m·K, while the IGBTs are made of silicon having a thermal conductivity of 120 W/m·K.

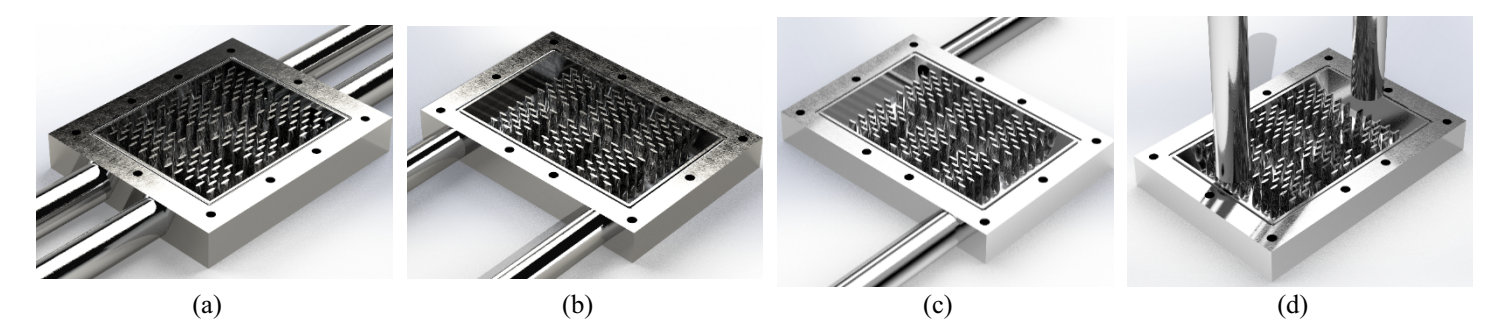


Fig. 1: 3D view of the heat sinks under study with different manifold positions: (a) new Dual, (b) M-shaped, (c) N-Shaped, (d) U-shaped.

3. Governing equations

The current study investigates the heat transfer and flow attributes of water flow inside the heat sink using a numerical approach. To this end, the governing equations are solved to assess the parameters such as temperature, velocity, and pressure. Some of the assumptions in solving the governing equations include a steady-state condition, negligible natural convection and thermal radiation, and a Newtonian fluid. Based on the above assumptions, the following equations are solved numerically in this research:

$$\frac{\partial}{\partial x_i} (\rho u_i) = 0 \tag{1}$$

$$\frac{\partial}{\partial x_{j}} \left(\rho u_{i} u_{j} \right) = -\frac{\partial p}{\partial x_{i}} + \frac{\partial}{\partial x_{j}} \left[\mu_{eff} \left(\frac{\partial u_{i}}{\partial x_{j}} + \frac{\partial u_{j}}{\partial x_{i}} - \frac{2}{3} \frac{\partial u_{k}}{\partial x_{k}} \right) \right]$$
(2)

$$\frac{\partial}{\partial x_i} \left(\rho u_i T c_p \right) = \frac{\partial}{\partial x_i} \left\{ \left(\lambda_f + \frac{c_p \mu_t}{P r_t} \right) \frac{\partial T}{\partial x_i} \right\}$$
(3)

$$\frac{\partial}{\partial x_i} \left(\lambda_s \frac{\partial T}{\partial x_i} \right) = 0 \tag{4}$$

Equations 1–4, respectively, show the conservation of mass, momentum, energy (water), and energy (heat sink). The effective viscosity in Eq. (4) can be defined as $\mu_{\it eff} = \mu_{\it t} + \mu$.

It is worth noting that the 4-equation SST turbulent model is utilized instead of the ordinary two-equation model to enhance the accuracy of the numerical simulations. The related transport equations can be found in [17].

4. Boundary conditions

The implemented boundary conditions in this study include (1) at the inlet: fully developed temperature and velocity profiles, (2) at the outlet: zero-gauge pressure, (3) contact regions: no-slip condition, and (4) outer surfaces: insulated.

5. Data processing

The average Nusselt number is:

$$\overline{Nu} = \frac{\overline{h}L_c}{k} \tag{5}$$

Where L_C denotes the characteristic length of the heat sink and is defined as:

$$L_c = \frac{2H_f S_T}{H_f + S_T} \tag{6}$$

where H_f and S_T respectively represent the pin fin height and spacing. And the friction factor:

$$f = \frac{2(\Delta P)L_c}{\rho U^2 L} \tag{7}$$

In the above equation, L is the length of the heat sink from the inlet to the outlet. Pumping power:

$$\dot{W} = \dot{V}\Delta P \tag{8}$$

Coefficient of variation:

$$CV = \frac{\sqrt{\sum_{i=1}^{N} (T_{b,i} - T_b)^2 / N}}{T_b}$$
 (9)

6. Numerical method and validation

The numerical analysis was conducted using the finite volume method implemented in ANSYS Fluent. The pressure-based solver was selected with the second-order upwind discretization. To model the pressure-velocity coupling, the SIMPLE technique is utilized. The convergence is obtained by monitoring the most important parameters, such as the temperature and pressure, with the residual criterion of 10^{-6} .

6.1. Grid sensitivity check

To ensure that the results are independent from the gird size, various gird sizes are evaluated, and the optimal gird is chosen for each manifold position. An unstructured polyhedral grid with $y^+\approx 1$ is employed in this research. Table 1 lists the grid sensitivity test results for different manifold positions at m=0.5 kg/s. As can be seen, both the Nu and f plateau when the grid cell number goes more than about 2.88, 3.38, 4.75, and 3.56 million cells for Dual, N–, M–, and U–shaped, respectively. As refining the grid more than the mentioned cell numbers result in inconsequential changes in both f and Nu, it can be concluded that the gird cell numbers highlighted in the table are the optimal grid sizes for this study. It is worth noting that the grid test is conducted at heat flux of 200 W/cm² and mass flow rate of 0.5 kg/s.

Dual M-shaped U-shaped N-shaped Cell No. NuCell No. NuCell No. Nuf Cell No. Nu569204 210.5 2.44 698713 169.1 0.98 509254 185.4 0.77677091 174.2 1.01 1149001 198.1 2.78 1255572 152.6 1.34 1088366 180.2 0.87 1155090 166.3 1.29 1987333 192.8 3.13 2033861 149.4 1.48 1907651 175.1 0.99 2003011 160.9 1.62 2879909 190.7 3.37 3387006 146.4 1.51 3`490066 172.3 1.18 3563791 158.3 1.71 4769111 190.5 3.39 5811092 146.3 1.50 4752040 169.8 1.22 7256001 158.1 1.70 7906545 190.4 3.41 9331066 1.49 8311777 169.6 1.23 8966890 158.0 1.71 146.1

Table 1: Grid sensitivity results for different manifold positions at $\dot{m} = 0.5$ kg/s.

11264422

169.5

1.23

6.2. Validation

The validation of the present numerical method is accomplished by comparing the results achieved using the current numerical technique with those reported by the experimental work of Choudhary et al. [18]. The validation of the current study was based on the Nusselt number and friction factor of water flowing through a pin fin heat sink with circular fins. The pin fins were arranged in a staggered configuration, consistent with the present investigation. The turbulent water-flow regime is also relevant. The pin fin pitch ratio was 2, and the pin fin diameter was 10 mm. The validation results are listed in Table 2. The numerical approach employed in this study is deemed reliable and valid because the calculated deviations are within an acceptable range.

Re	Choudhary et al. [18]	Present study Nu	Deviation	Choudhary et al. [18]	Present study	Deviation
7000	423	437.0	-3.30%	0.287	0.269	6.3%
9000	439.5	457.9	-4.19%	0.192	0.181	6.0%
11000	465	484.2	-4.14%	0.141	0.129	9.0%
13000	492	515.9	-4.86%	0.119	0.117	2.2%
15000	528	555.0	-5.10%	0.098	0.089	9.2%

Table 2: Validation results.

7. Results and discussion

The average Nusselt number in terms of the coolant mass flow rate is delineated in Fig. 2 for different manifold inlet/outlet positions. As the figure shows, the lowest Nusselt number is achieved by the N-shaped case, while the highest Nusselt number belongs to the new Dual manifold layout. The U- and M-shaped layouts stand in between the Dual and the N-shaped. Considering the N-shaped layout as the baseline due to its lowest performance, the enhancement rates obtained using other manifold layouts are noted in front of each. Obviously, the Dual manifold layout increases the Nusselt number by up to 43% and in most cases, its improvement rate is almost twice that of the M-shaped, reflecting a significant better heat transfer performance.

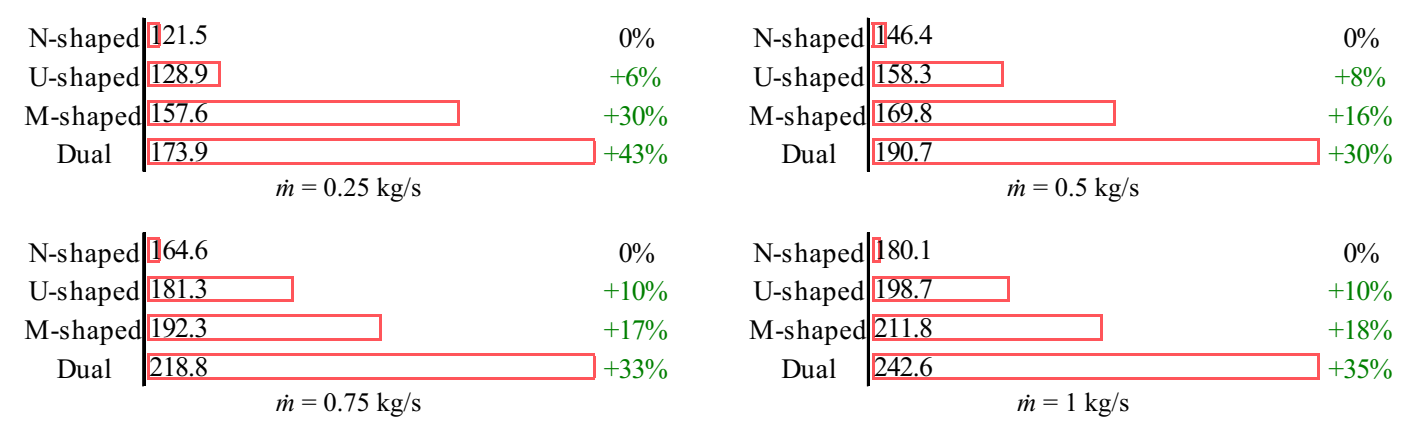


Fig. 2: Comparison between the average Nusselt numbers of different manifold locations for various mass flow rates.

Fig. 3 demonstrates the IGBT temperatures obtained using different manifold layouts for different mass flow rates. Moreover, the corresponding coefficient of variation for each case is also shown in Fig. 3. As can be seen, the IGBTs in the case of the new Dual manifold not only experience the lowest temperature but also benefit from the more even temperature distribution over the entire baseplate. A closer look reveals that the temperature profile associated with the Dual manifold layout is by far the most even one among the other cases for all mass flow rates under study. The coefficient of variation that is highlighted in this figure for each case and mass flow rate underpins this fact and demonstrates significantly better

performance that is achieved with the new dual design. From the figure, the coefficient of variation drops up to 75% compared to the baseline N-shaped layout, using the new Dual manifold layout, which is about 20% better than the M-shaped. As a result, it can be concluded that the higher heat transfer capability observed in Fig. 2 is evenly distributed, which in turn can reduce the generation of local hot spots.

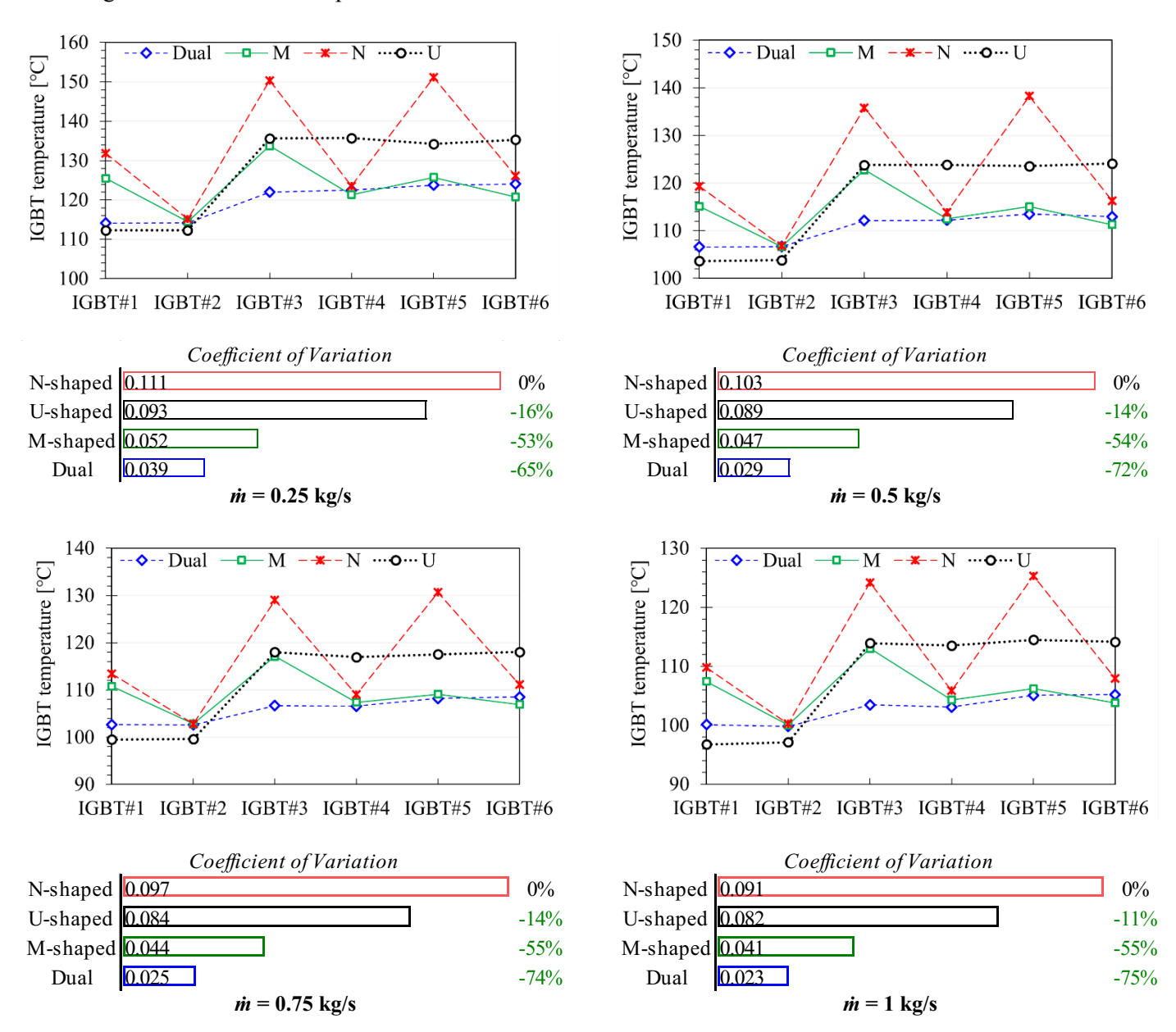


Fig. 3: Comparison between the IGBT temperature obtained using different manifold layouts for various mass flow rates along with the corresponding coefficient of variation for each case.

Fig. 4 shows the temperature and the velocity contours over different cross sections of the heat sink for various manifold layouts. These figures underpin the previous results, and the IGBTs in the case of Dual manifold are shown to experience a lower and more even temperature than in other cases. Using the velocity contours, the uniformity of temperature can be

explained by how the coolant flow navigates through the pin fins more efficiently with the Dual manifold. In contrast, the N– and M–shaped manifolds cause flow misdistribution across the pin fins. However, in the case of the M–shaped manifold, the flow navigation through the pin fins occurs in a more effective way than the N– and U–shaped ones. This also explains the superior performance of the M–shaped manifold compared to U– and N–shaped ones.

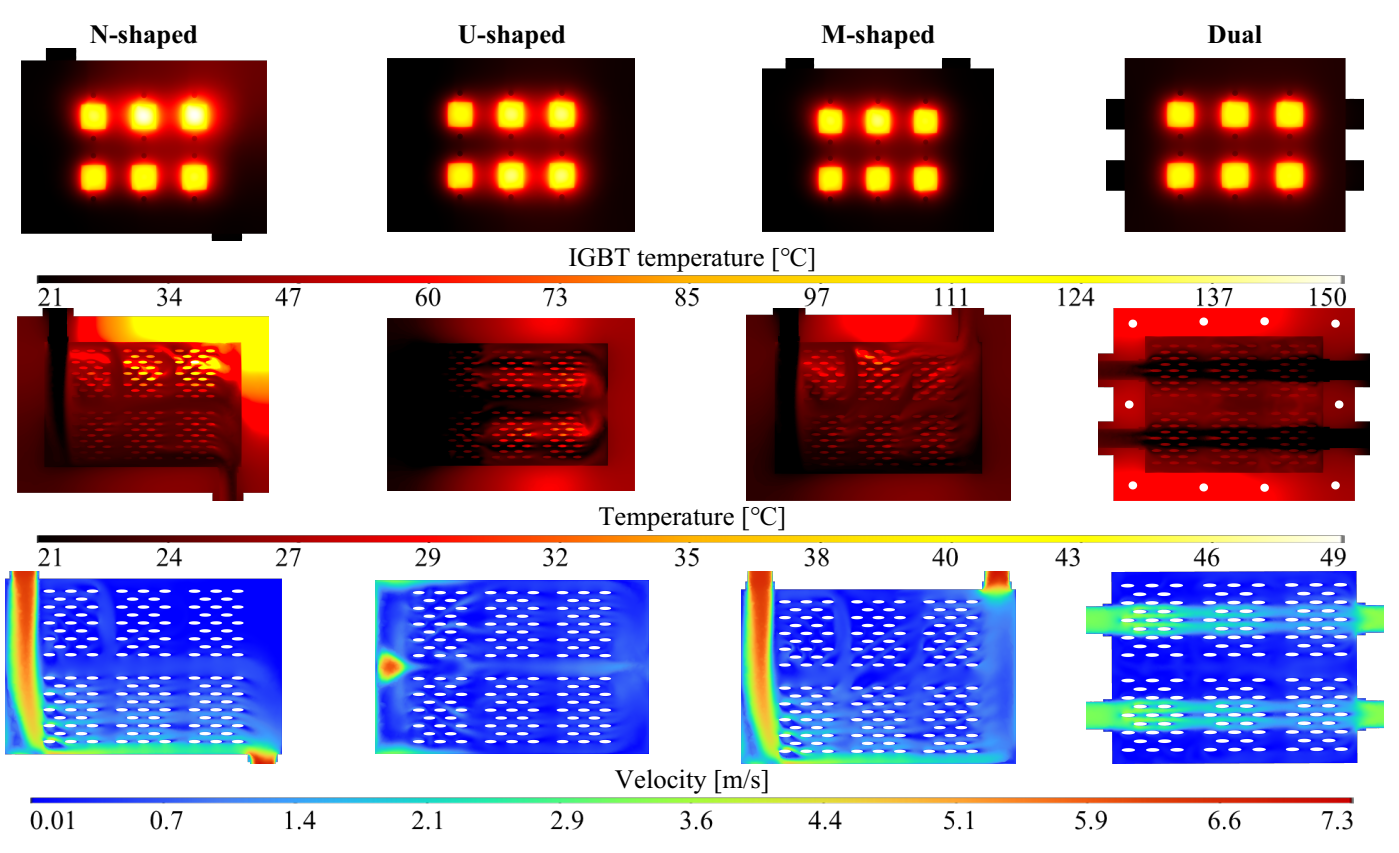


Fig. 4: Temperature and velocity contours over different sections of the heat sink for various manifold layouts.

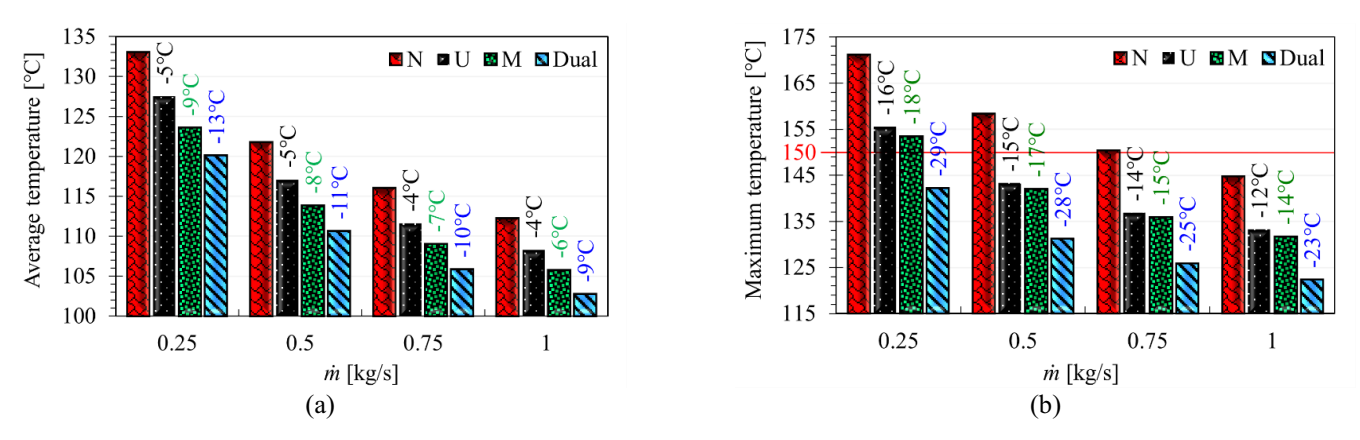


Fig. 5: (a) the average and (b) maximum temperatures of the baseplate versus the coolant mass flow rates.

Fig. 5 illustrates the maximum and the average temperatures of the heat sink's baseplate versus the water mass flow rate for different manifold layouts. The temperature changes of each case with respect to the N-shaped manifold are also highlighted over each bar. The figure shows considerable better performance of the Dual manifold as it lowers the maximum temperature by about 29°C that saves the IGBT from overheating. All in all, the U- and the M-shaped are close, but the Dual manifold outperforms these two cases by providing a superior cooling efficiency and lower average and maximum temperatures.

The required pumping power for different cases and mass flow rates is presented in Fig. 6. It can be understood that the cost of having a Dual manifold is significantly high indeed, with 119%–142% higher pumping power than the N–shaped manifold. This is attributed to the flow expansion and contraction caused by multiple inlets/outlets. The flow pathline visualizations are also presented for different cases in Fig. 7 to support this statement.

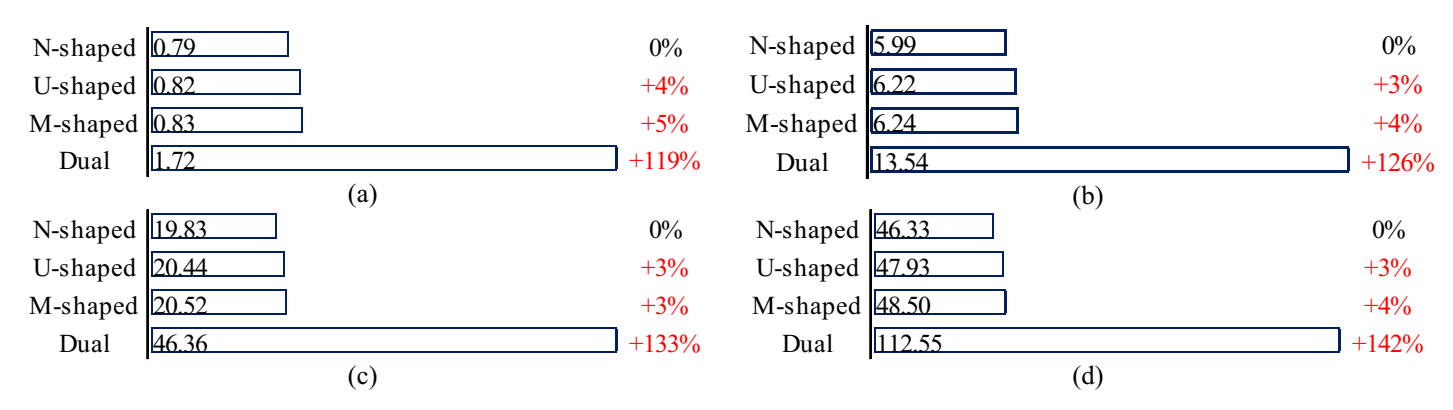


Fig. 6: Required pumping power [W] for different manifold layouts and mass flow rates.

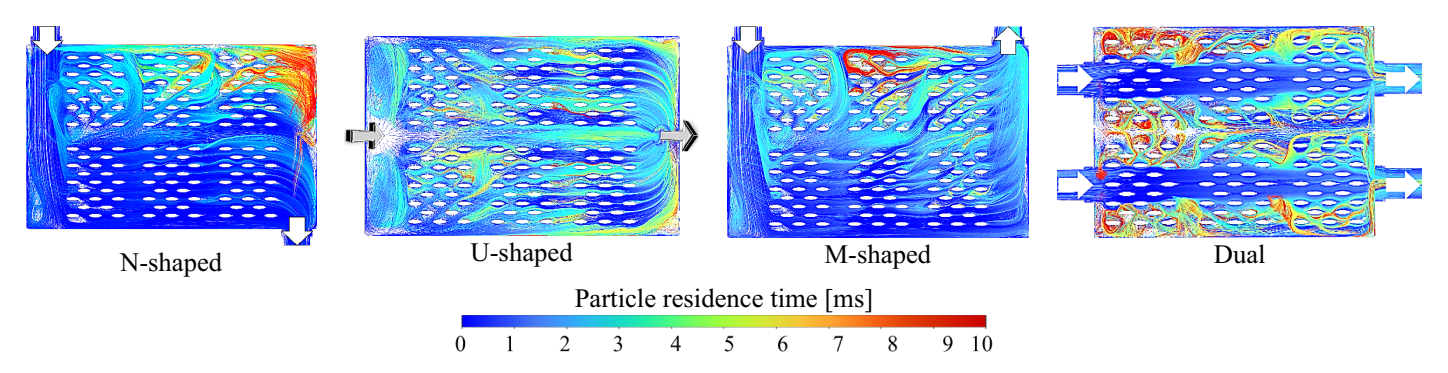


Fig. 7: Comparison between the flow pathlines for different manifold layouts at $\dot{m} = 0.5$ kg/s.

Even though the Dual manifold consumes a considerably higher amount of energy to provide a superior cooling performance at a constant mass flow rate, it outperforms others at a constant pumping power. Fig. 8 compares both the IGBT temperatures and their corresponding coefficient of variations of different manifold layouts at the constant pump power of 13.5 W. As can be seen, even though the M-shaped manifold provides a lower IGBT temperatures in some cases, its coefficient of variation is as twice as high as the Dual one. This suggests less thermal cycling and a more reliable cooling by preventing the presence of hot spots over the baseplate. The Dual manifold design, as depicted in Fig. 7, effectively concentrates the flow over the pin fins, resulting in enhanced cooling performance. Furthermore, the presence of two inlets/outlets aligned with each other reduces the distance the flow must travel, thereby preventing the thermal boundary

layer from growing as thick as in other configurations. Consequently, a thinner thermal boundary layer also contributes to an increased heat transfer rate.

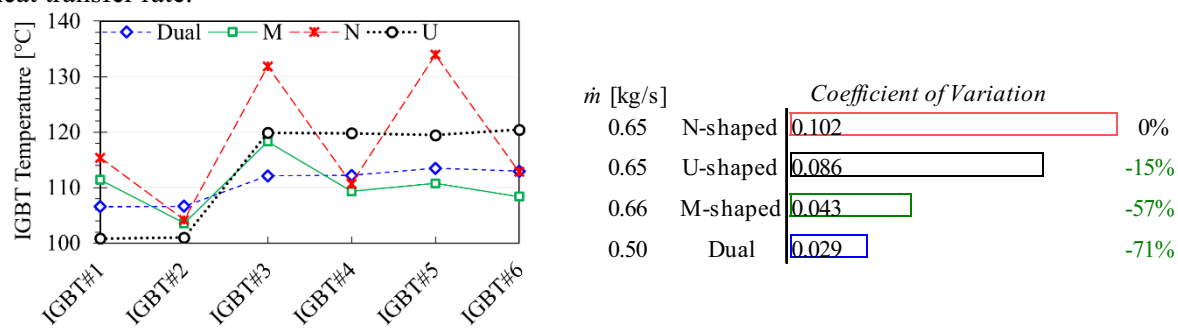


Fig. 8: Comparison between the IGBT temperatures of different manifold layouts at constant pumping power of 13.5 W along with the corresponding coefficient of variations.

8. Conclusion

The present investigation explored the effects of manifold positioning on the hydrothermal features of water within a topology-optimized pin-fin heat sink for thermal management of power inverters embedded in EVs/HVs. Four different manifold types, i.e., M– and N–, U-shaped, and a new Dual were investigated at various mass flow rates and a constant heat flux of 200 W/cm². Results showed that the new Dual manifold can achieve up to 43% higher heat transfer rate compared to the N–shaped one, while the pump power rises by 119%. Moreover, the temperature uniformity obtained by the Dual manifold was 75% better than the N–shaped one. At a constant pumping power, the Daul manifold outperforms other counterparts, especially when it comes to temperature uniformity. This study makes a significant contribution to the development of sustainable transportation solutions and the advancement of electric mobility by improving the thermal management of high-heat flux components in EVs/HVs.

Acknowledgements

We acknowledge the support of the Volt-Age Seed Grant 2023 by the University of Concordia under the Canada First Research Excellence Fund. The support from the Schulich School of Engineering at the University of Calgary is also duly acknowledged and appreciated. The authors also gratefully acknowledge the support of the University of Calgary through the Faculty of Graduate Studies Doctoral Scholarship and the Provost's Doctoral Scholarship.

References

- [1] International Energy Agency (IEA), *Executive Summary Global EV Outlook 2025* [Online]. Available: https://www.iea.org/reports/global-ev-outlook-2025/executive-summary (accessed Jun. 2, 2025).
- [2] European Alternative Fuels Observatory, *Homepage* [Online]. Available: https://alternative-fuels-observatory.ec.europa.eu/ (accessed Sep. 29, 2024).
- [3] J. Vetrovec and A. Litt, "Progress in the development of a high-performance heat sink for hybrid electric vehicle inverters," *SAE Int. J. Altern. Powertrains*, vol. 1, pp. 89–96, 2012. doi: 10.4271/2012-01-0339.
- [4] N. Mazaheri and A. Mwesigye, "Application of novel double-layer micro-jet heat sinks for energy-efficient thermal management of motor inverters in electric vehicles," *Appl. Therm. Eng.*, 2023, Art. no. 120836. doi: 10.1016/j.applthermaleng.2023.120836.
- [5] B. Li, H. Kuo, X. Wang, Y. Chen, Y. Wang, D. Gerada, S. Worall, I. Stone, and Y. Yan, "Thermal management of electrified propulsion system for low-carbon vehicles," *Automot. Innov.*, vol. 3, pp. 299–316, 2020. doi: 10.1007/s42154-020-00124-y.
- [6] Reddit, "Tesla inverter overheating," r/TeslaSolar, [Online]. Available:
 - https://www.reddit.com/r/TeslaSolar/comments/nqt14d/tesla_inverter_overheating/ (accessed Dec. 9, 2024).
- [7] Reddit, "Tesla new inverter overheating and causing intermittent production," *r/TeslaSolar*, [Online]. Available: https://www.reddit.com/r/TeslaSolar/comments/x52px8/tesla new inverter overheating and causing/ (accessed Dec. 9, 2024).

- [8] Y. Cai, D. Liu, F. Y. Zhao, and J. F. Tang, "Performance analysis and assessment of thermoelectric micro cooler for electronic devices," *Energy Convers. Manag.*, vol. 124, pp. 203–211, 2016. doi: 10.1016/j.enconman.2016.07.011.
- [9] J. Jaguemont, L. Boulon, and Y. Dubé, "A comprehensive review of lithium-ion batteries used in hybrid and electric vehicles at cold temperatures," *Appl. Energy*, vol. 164, pp. 99–114, 2016. doi: 10.1016/j.apenergy.2015.11.034.
- [10] Y. Zhang, X. Liu, W. Wei, T. Peng, G. Hong, and C. Meng, "Mobile charging: A novel charging system for electric vehicles in urban areas," *Appl. Energy*, vol. 278, Art. no. 115648, 2020. doi: 10.1016/j.apenergy.2020.115648.
- [11] N. Mazaheri and A. Mwesigye, "Novel high heat flux thermal management with combined supercritical CO₂ and a microjet heat sink," *Appl. Therm. Eng.*, vol. 256, Art. no. 124143, 2024. doi: 10.1016/j.applthermaleng.2024.124143.
- [12] P. Bhandari, K. S. Rawat, Y. K. Prajapati, D. Padalia, L. Ranakoti, and T. Singh, "Design modifications in micro pin fin configuration of microchannel heat sink for single phase liquid flow: A review," *J. Energy Storage*, vol. 66, Art. no. 107548, 2023. doi: 10.1016/j.est.2023.107548.
- [13] M. Bahiraei, N. Mazaheri, and M. R. Daneshyar, "Employing elliptical pin-fins and nanofluid within a heat sink for cooling of electronic chips regarding energy efficiency perspective," *Appl. Therm. Eng.*, vol. 183, Art. no. 116159, 2021. doi: 10.1016/j.applthermaleng.2020.116159.
- [14] F. Han, H. Guo, and X. Ding, "Design and optimization of a liquid cooled heat sink for a motor inverter in electric vehicles," *Appl. Energy*, vol. 291, Art. no. 116819, 2021. doi: 10.1016/j.apenergy.2021.116819.
- [15] K. Zhao, X. Sun, Y. Xia, Q. Li, L. Shen, and M. Lin, "Cooling performance in a minichannel heat sink with different triangular pin-fins configurations," *Front. Energy Res.*, vol. 11, Art. no. 1087501, 2023. doi: 10.3389/fenrg.2023.1087501.
- [16] G. Qian, X. Dou, G. Lu, H. Liu, Q. Wu, R. Jiang, R. Huang, Z. Li, and X. Yu, "Parametric study and design of liquid cooling plates for high power density IGBT modules in wind power generation systems," *Therm. Sci. Eng. Prog.*, vol. 43, Art. no. 101992, 2023. doi: 10.1016/j.tsep.2023.101992.
- [17] M. Bahiraei, N. Mazaheri, M. R. Daneshyar, and A. Mwesigye, "Two-phase simulation of irreversibilities for Ag—water nanofluid flow inside an elliptical pin-fin heat sink: Entropy generation and exergy considerations," *Powder Technol.*, vol. 409, Art. no. 117723, 2022. doi: 10.1016/j.powtec.2022.117723.
- [18] V. Choudhary, M. Kumar, and A. K. Patil, "Experimental investigation of enhanced performance of pin fin heat sink with wings," *Appl. Therm. Eng.*, vol. 155, pp. 546–562, 2019. doi: 10.1016/j.applthermaleng.2019.03.139.